Composites Part A 130 (2020) 105734

Contents lists available at ScienceDirect

Composites Part A

journal homepage: www.elsevier.com/locate/compositesa

Identification of process-induced residual stresses in 3D woven carbon/epoxy composites by combination of FEA and blind hole drilling

Kostiantyn Vasylevskyi[a,*], Igor Tsukrov[a], Borys Drach[b], Hilary Buntrock[a], Todd Gross[a]

[a] University of New Hampshire, Durham, NH 03824, USA
[b] New Mexico State University, Las Cruses, NM 88003, USA

ARTICLE INFO

Keywords:
A. Fabrics/textiles
A. 3-Dimensional reinforcement
B. Residual/internal stress
C. Finite element analysis (FEA)

ABSTRACT

Process-induced residual stresses in 3D woven carbon-epoxy composites are studied by blind hole drilling experiments interpreted with finite element (FE) modeling. It is assumed that residual stresses are primarily caused by the difference in thermal expansion coefficients of the constituents which are modelled as temperature-dependent linear elastic solids. The impact of residual stresses is quantified by drilling blind holes in the composite panels and mapping the resulting in-plane surface displacements by electronic speckle pattern interferometry. Mesoscale finite element models are used to correlate these surface displacements with the volumetric distribution of the residual stresses in the composite. This is done by determining the effective temperature drop ΔT^{eff} that results in the same predictions for the surface displacements as experimentally measured. The effective temperature drop approach allows to use linear elastic models while approximately accounting for various nonlinear effects occurring in the material during processing. The models are also used to establish the sensitivity of the predicted results to the exact location of a hole and its depth.

1. Introduction

Manufacturing-induced residual stresses in carbon epoxy composites can occur due to the difference between coefficients of thermal expansion (CTE) of the resin and fibers and also chemical shrinkage [1], compaction of the resin [2], nonlinear distribution of temperature and degree of cure throughout the part during curing, etc. It has been shown that the level of residual stresses can substantially affect the quality and performance of the composite parts including their final shape [3,4] and strength [5,6].

A significant amount of publications have been devoted to the manufacturing-induced residual stresses in laminated and 2D woven composites. For example, Cowley and Beaumont [3] carried out experimental study on the residual stresses in the laminated fibrous polymers and modeled the stress state using classical lamination theory. Golestanian and El-Gizawy [7] simulated the entire curing and cooling cycle for the woven carbon and fiberglass mats impregnated with epoxy resin using resin transfer molding (RTM). They obtained values for the residual stresses in the selected points of the composite plate. Fiedler et al. [8] investigated the influence of the manufacturing-induced thermal residual stress on the transverse strength of the unidirectional CFRP composite material. Agius et al. [9] performed FE simulations to predict residual stresses in the multidirectional laminates based on the epoxy resin chemical shrinkage and mismatch in CTEs of the epoxy and carbon fiber reinforcement. Benavente et al. [10] simulated macroscopic residual deformation of a laminate composite part based on the temperature-dependent viscoelastic epoxy resin behavior.

In 3D woven composites, presence of additional constraints in the third direction leads to higher residual stresses from mismatch of CTEs of the fiber and matrix. It has been shown in [11] that for certain reinforcement architectures manufacturing-induced residual stresses might lead to significant levels of residual stresses causing microcracking in the resin pockets between the tows.

Determining the residual stress distribution in 3D woven composites experimentally is challenging due to their complex microstructure and the resulting high level of inhomogeneity and anisotropy. One of the approaches to estimate residual stresses is to utilize hole drilling experiments. In such experiments, the residual stresses are estimated based on the displacements around a circular hole drilled in the material, as described in [12,13]. However, this purely experimental approach developed for homogeneous materials does not allow to obtain a detailed distribution of the residual stress in woven composites. There is a need to numerically interpret the measurement results. For example, Pisarev et al. [14] proposed to use analytical solutions given in [15] to correlate residual stresses with the displacements due to the through-thickness holes drilled in the composite plates. They measured the

* Corresponding author.
E-mail address: kv1012@wildcats.unh.edu (K. Vasylevskyi).

https://doi.org/10.1016/j.compositesa.2019.105734
Received 11 July 2019; Received in revised form 14 December 2019; Accepted 17 December 2019
Available online 17 December 2019
1359-835X/ © 2019 Published by Elsevier Ltd.

displacements using electronic speckle pattern interferometry (ESPI) and assumed composite material to be homogeneous and orthotropic. Akbari et al. [16] obtained residual stress in a filament wound laminated carbon/epoxy ring using incremental hole drilling method. In their study, they used a combination of strain gage measurements and finite element simulations to obtain the in-plane residual stresses in the plies assuming the material of each ply to be homogeneous and orthotropic. Wu et al. [17] estimated residual stresses in 2D woven composite utilizing a combination of FE modeling and Moiré interferometry. In their study, they assumed a uniform distribution of stress within the material removed during drilling to produce the values of residual stress components based on the measured displacements at the sample points on the composite plate surface around the drilled hole.

In the present paper, we estimate residual stresses in 3D woven composites using measurements of displacements on the surface of the composite panels caused by drilling of circular blind holes in various locations. The displacements can be measured utilizing either ESPI or digital image correlation (DIC) techniques. In our previous studies we determined that ESPI provided better resolution of the displacement gradients [18] so it was selected for the present work. The displacements are correlated to the residual stress by mesoscale finite element models of the composites. These models assume that the primary mechanism of the residual stress formation is the mismatch in CTE of fiber and matrix as the composite cools from curing to room temperature.

The rest of the paper is organized as follows. Section 2 provides a description of the experimental techniques utilized in this work. Section 3 describes the numerical modeling procedure and also includes information on mechanical properties of the composite phases. Section 4 presents the results of numerical parametric studies related to the hole drilling experiment. Section 5 provides interpretation of the hole drilling experiments by FEA to obtain the full residual stress field in 3D woven composites. Section 6 contains concluding remarks and comments.

2. Experimental methods

Experimental measurements were conducted on 4 mm thick composite panels fabricated by Albany Engineered Composites using Hexcel RTM6 resin and Hexcel 12K IM7 PAN-based carbon fibers. Two different levels of through-thickness reinforcement were considered: one-by-one orthogonal (significant through-thickness reinforcement) and ply-to-ply (low through-thickness constraint). The materials had an overall reinforcement volume fraction of 68.96% and 68.74% for orthogonal and ply-to-ply respectively. More detailed information on the considered reinforcement architectures is shown in Table 1.

The composite sections (of sufficient in-plane dimensions to avoid boundary effects) were cut from the panels and painted with white, high heat spray paint. The black speckles were applied using an airbrush to get speckles that ranged in size from 5 to 10 μm. Then the surface was covered with a clear matte spray paint to protect the speckles from drilling debris deposits and prevent the speckles being removed with the water used for cooling during drilling. The sample was glued on a block mounted on a Thor Labs kinematic mount to allow precise repositioning of the “before drilling” and “after drilling” interferograms. The apparent placement repeatability was on the order of 5 μm or less.

Table 1
Weave architectures under investigation. The Warp V_f and Weft V_f columns list the volume fractions of the warp and weft reinforcement tows in the composite estimated using an idealized geometry.

Architecture	Filaments Per Tow	Picks Per Inch	Pattern	Frames	Warp Vf	Weft Vf
Ply-to-ply	12 K	12 × 10	ply-to-ply	4	36.16%	32.58%
Orthogonal	12 K	10 × 10	orthogonal	2	36.37%	32.58%

Residual stresses were studied by drilling a 1 mm diameter blind hole to a depth of 0.5 mm and recording the resulting in-plane displacements on the surface of the specimen. Drilling was done with UKAM diamond coring tool. The depth was continuously measured with a dial indicator attached to the drilling head. A continuous flow of deionized water was manually applied during drilling using a squeeze bottle. The water was used to minimize the heat generated during drilling and to carry away the drilling debris. The sample was rinsed with more water after drilling and dried with a flow of warm air.

The in-plane displacements around the hole were measured using a custom-built electronic speckle pattern interferometry system similar to the one described by Díaz et al. [19]. A 50 mW Melles Griot HeNe laser with linear polarization was used. The angle between the normal to the specimen and the illumination beams was 45^o which resulted in a 448 nm displacement for a phase difference corresponding to 2π. The system exhibited phase noise of $<\pi/25$ which corresponds to a displacement of approximately 9 nm.

3. Numerical models on mesoscale

3.1. Model development. Reinforcement architecture

Due to the periodicity of the woven composites reinforcement, a numerical model of the smallest repeatable portion of the material – the unit cell (UC) was created. As described in [20], the modeling process begins with material reinforcement geometry development. There are several numerical approaches to obtain a geometrical representation of the material reinforcement that have been utilized in [21,22,23,24]. In our research we used Digital Fabric Mechanics Analyzer (DFMA), see [25]. The selection of the DFMA modelling parameters was informed by μCT scanning to accurately reproduce the reinforcement shape and volume fraction, see [26]. Fig. 1 presents FE models of unit cells of the two reinforcement architectures considered in this paper.

Once the reinforcement mesh was created, the epoxy resin phase finite element representation was obtained by meshing the space between the tow surfaces and borders of the unit cell. The resulting models consisted of 558,587 tetrahedral elements for orthogonal and 5,548,316 for ply-to-ply reinforcement architecture. The unit cells included the entire thickness of the test panels ($t = 4mm$); their in-plane dimensions were 5.08×5.08 mm^2 for the orthogonal and 10.16×8.467 mm^2 for the ply-to-ply architectures.

Mesoscale simulations of woven composites are usually conducted for unit cells with periodic boundary conditions, e.g. [27,22,28]. However, if such conditions are used in the hole drilling modeling, the displacement fields resulting from the release of the residual stress around the hole are assumed to be present periodically in the material. To avoid this periodic boundary effect, the model should include several adjacent unit cells. Our parametric studies showed that 3×3 model is sufficient even when the hole is located close to the boundary of the central UC. However, modeling of nine unit cells requires significant time and computational resources. We compared the results for 3×3 UC model, two models of a single UC (with and without periodic boundary conditions), and a model with one unit cell surrounded by the homogeneous material with effective properties of the composite. Note that usage of the homogeneous material does not require such a refined mesh as an actual unit cell while representing the material behavior around the UC under consideration. The effective material approach turned out to be the best compromise to analyze the entire composite specimen described in Section 2 with reasonable computational effort, see [29].

3.2. Mechanical properties of the composite phases

In our simulations we assumed the matrix to be fully cured and behaving elastically. The accuracy of this assumption is discussed in

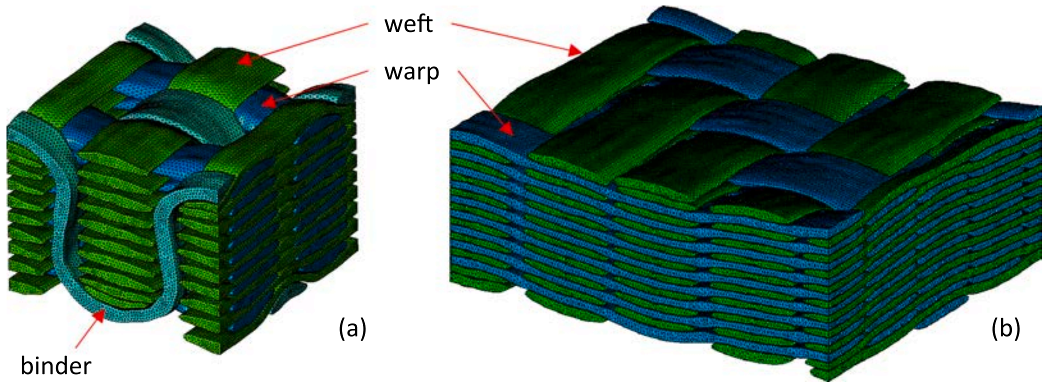

Fig. 1. FE representation for (a) orthogonal and (b) ply-to-ply reinforcement architectures consisting of weft, warp and binder tows. (For interpretation of the references to colour in this figure legend, the reader is referred to the web version of this article.)

Section 5. The matrix (HEXCEL RTM6 epoxy resin) was simulated as an isotropic material with constant Poisson's ratio $\nu_m = 0.35$ and temperature dependent Young's modulus E_m and thermal expansion coefficient α_m:

$$E_m = E_m^{0^\circ C} - \beta_m T \tag{1}$$

$$\alpha_m = \alpha_m^{0^\circ C} + \gamma_m T \tag{2}$$

where T is the temperature in °C, and $E_m^{0^\circ C} = 3,500\,\text{MPa}$, $\beta_m = 5.9\frac{MPa}{^\circ C}$, $\alpha_m^{0^\circ C} = 5\times10^{-5}\frac{1}{^\circ C}$, $\gamma_m = 1.05\times10^{-7}\frac{1}{(^\circ C)^2}$ are the material parameters chosen to reproduce the experimental results reported in [30]. The tows (12K IM7 carbon fibers impregnated with RTM6 epoxy) were simulated as transversely isotropic materil with the properties obtained by micromechanical modeling described in [31]. The numerical values are provided in Table 2. The values are provided assuming direction 1 is parallel to the axis of the tow and directions 2 and 3 are transverse to the tow axis. Note that even though the properties of the matrix in the tows change with temperature as given by formulas (1) and (2), these changes will result in insignificant variations of the homogenized properties of the tows (see comparison in [31]), so in the numerical simulations the properties of the tows were assumed to be temperature independent.

3.3. Modeling of cooling after curing and hole drilling

The simulations were conducted using MSC Marc FE software (see http://www.mscsoftware.com/product/marc/) in two steps. First, the simulation of cooling after complete curing with the temperature drop from 165 °C (temperature when the resin is fully cured) to room temperature of 25 °C was performed. This simulation resulted in accumulation of the residual stresses. The second step was the drilling simulation which was accomplished as follows: finite elements corresponding to the material removed by drilling were chosen manually at the model preprocessing stage and stored as a custom element set. These elements were deactivated (using MSC Marc "Deactivation" feature which removes a chosen set of finite elements) after the cooling loadcase resulting in the displacements due to release of the residual stress by the removal of the material.

4. Numerical modeling studies using linearly elastic model of cooling

Even though we neglect viscoelastic and plastic effects that can be significant, the linear elastic approach allows us to quantitatively investigate sensitivity of the results to FE meshing, the depth of the hole, and its location with respect to the composite reinforcement. Note that a simple and efficient procedure to adjust the results to more realistic nonlinear estimates of residual stresses is presented in Section 5.

4.1. Hole edge meshing sensitivity

Since finite elements corresponding to the drilled hole are chosen manually from the automatically generated mesh, the edge of the hole in the model might not be smooth due to the fact that the hole location is unknown at the mesh generation step. This issue can be overcome by incorporating the location of the hole into mesh generation process so that the hole edges are modeled as smooth surfaces (see Fig. 2). However, this causes additional complications in the meshing procedure and makes the model a single-use for one particular hole. In order to investigate how the smoothness of the edge affects the results of the simulation, we compared predictions for the ply-to-ply architecture presented in Fig. 1(b). Two hole locations were chosen for the comparison as shown in Fig. 2(a). Both of the holes were modeled using both automatically and specifically generated meshes, see Fig. 2(b) and (c). The images (b) and (c) represent the hole edge resulting from automatic meshing technique (rough) and the edge specifically generated for a prescribed hole location (smooth).

To compare the results, the displacements after hole drilling were captured on the surface of the unit cell along the lines shown in Fig. 2(a). Fig. 3 presents the displacements in the warp (X) direction plotted along horizontal lines and the displacements in the weft direction (Y) plotted along the vertical lines, correspondingly. In this figure and all the slice plots thereafter the X and Y coordinates are given in the local coordinate system with the origin in the center of the hole. As can be seen, there are no significant differences in the predicted displacements between two meshing techniques. Slight deviations are observed only at the very edges of the holes. However, for the purpose of interpreting the experimental drilling results these deviations are not critical because in the experimental measurements, the surface of the specimen near the edge of the hole is within the decorrelated zone ($180\mu m$around the edge) where the exact experimental results are not

Table 2
Elastic properties of the tows.

Material Combination	E_{1t} (GPa)	E_{2t} (GPa)	G_{12t} (GPa)	ν_{12t}	ν_{23t}	α_{1t} (1/K)	α_{2t} (1/K)
IM7 fibers + RTM6 epoxy	221.38	13.18	7.17	0.35	0.35	−2.29E-7	2.23E-5

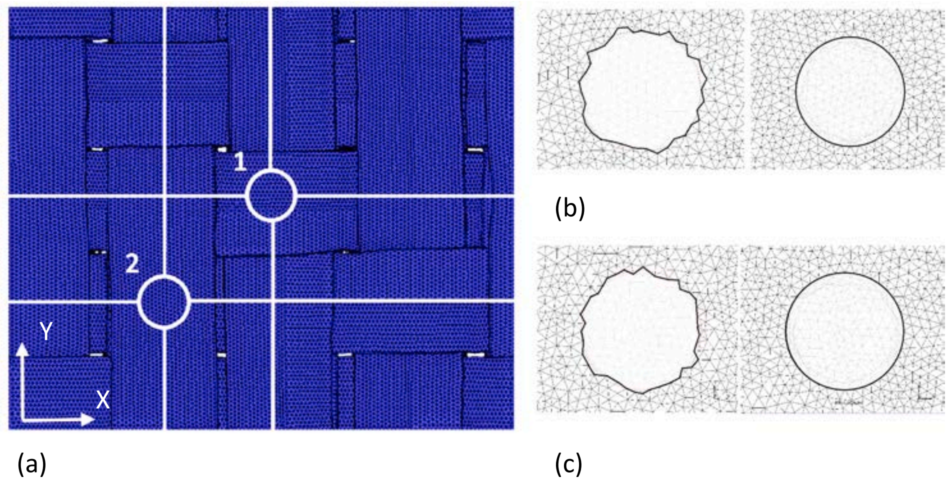

Fig. 2. (a) Locations of the holes chosen to investigate the hole edge meshing sensitivity. Finite element meshes around (b) hole 1 and (c) hole 2. (For interpretation of the references to colour in this figure legend, the reader is referred to the web version of this article.)

available. Thus, there is no need to generate specific meshes for particular hole locations for the hole drilling interpretation analysis. In the rest of the presented simulations we used the automatically generated meshes with "rough" hole edges.

4.2. Hole location influence

Due to the same dimensional orders of the drilled hole and the reinforcement features, it is important to understand how the exact location of the hole with respect to the reinforcement affects the displacement fields. To estimate the impact of the hole location a set of simulations was performed. Both orthogonal and ply-to-ply reinforcement architectures were considered. The hole locations were chosen as shown in Fig. 4. All of the holes are of the same depth $H = 0.5$ mm and diameter $D = 1$ mm. Similarly to the hole edge meshing study, the displacements along the vertical (Y) and horizontal (X) slice lines through the center of each hole are plotted.

In the interpretation of the simulation results, we hypothesize that the residual stresses due to the cooling after curing will mostly be tensile for the resin as it is prevented from shrinking by the constraints of carbon fiber tows. For the tows, especially warp and weft, we expect the stress to be tensile transversely to the tow axis (pulled by adjacent resin). The distribution in the directions longitudinal to the tow axis is expected to be more complex as it will be influenced by interaction with neighboring tows. Most of the warp and weft tows are expected to be in longitudinal compression. These hypotheses are checked by FEA simulations in this section, and the comparison with experimental observations presented in Section 5

For each hole location, the cooling of completely cured composite was simulated with the temperature drop of $\Delta T = -140$ °C (from 165 °C to 25 °C). Then the finite elements corresponding to the material occupied by the hole were deactivated to simulate the material removal due to the drilling and nodal displacements were recorded. The displacements along slice lines for each hole location were superimposed to evaluate the sensitivity of the results to the hole location. The results are presented in Figs. 5 and 6 for orthogonal reinforcement and Figs. 7 and 8 for ply-to-ply. Note that some of the presented curves exhibit rapidly increasing/decreasing behavior near the hole edge. This effect is

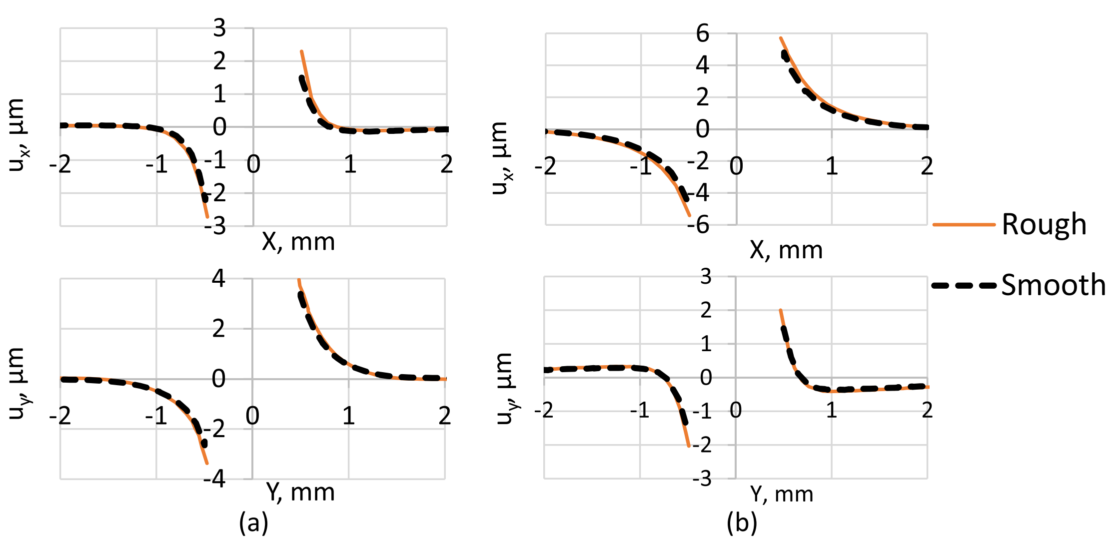

Fig. 3. Slice plots of the displacements in warp (u_x) and weft (u_y) directions for (a) hole location 1 and (b) hole location 2. (For interpretation of the references to colour in this figure legend, the reader is referred to the web version of this article.)

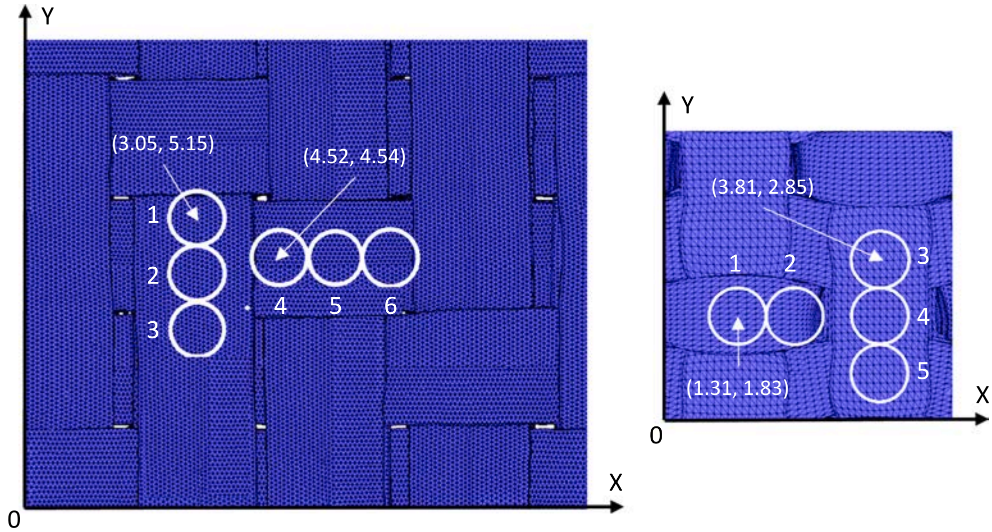

Fig. 4. Hole locations for the ply-to-ply (left) and orthogonal (right) architectures. Coordinates of hole centers within the unit cell are shown in millimeters. (For interpretation of the references to colour in this figure legend, the reader is referred to the web version of this article.)

numerical and caused by FEA discretization. In our estimate on whether the hole opens or closes due to release of the residual stress we used the stable portion of the curves 10–15 finite elements away from the edge.

Fig. 5 shows that the warp displacement field around the drilled hole is sensitive to its location. The highest sensitivity is observed in the case when the hole is moved along the center line of the binder tow. For the case depicted in Fig. 5, the horizontal slice lines for *hole* 1 and *hole* 2 locations are in the same direction as the binder tow being cut by these holes. According to the slice plots, *hole* 1 closes whereas *hole* 2 slightly opens and moves to the right towards the crossing weft top tow.

The warp displacements along the slice lines for the *holes* 3, 4 and 5 are similar to each other. *Hole* 4, however, shows more pronounced opening. This phenomenon can be explained by the microstructure of the reinforcement. All of these three holes cut the top weft tow, but *hole* 3 and *hole* 5 are located so that there are crossing warp tows underneath the weft being cut. Due to the compressive residual stress in the tows along their central lines, when the tow is cut the hole would close in the direction along the tow. This phenomenon can explain lower opening of the *hole* 3 and *hole* 5. *Hole* 4 in contrast is located in a way that there are no crossing tows underneath the top weft tow and hence its opening is more pronounced. It is also seen that the displacements are the same for *hole* 3 and *hole* 5 as expected from the reinforcement symmetry.

Fig. 6 shows weft (u_y) displacements along the slice line (as in Fig. 2(a)) for each hole location. *Hole* 1 and *hole* 2 open in the direction Y confirming the assumption that due to the tension stress in the matrix material, the drilled hole opens transversely to the tow (binder in this particular case). Three other holes close in Y direction which confirms the presence of the compressive residual stresses in the tows along their central lines.

The same numerical study was performed for the ply-to-ply reinforcement architecture. Six hole locations were considered, three of them cut the weft tow and the other three - the warp. Fig. 7 shows warp (along X-axis) slice displacements. A certain sensitivity to the hole location is observed for *holes* 4–6, whereas the displacements caused by *holes* 1–3 are location-insensitive. *Holes* 4 through 6 cut the warp tow and show slight closure in X direction. This behavior is dictated by the compressive residual stress in the tow along its central line. However, when the hole is located near the crossing weft (such as *hole* 4), in

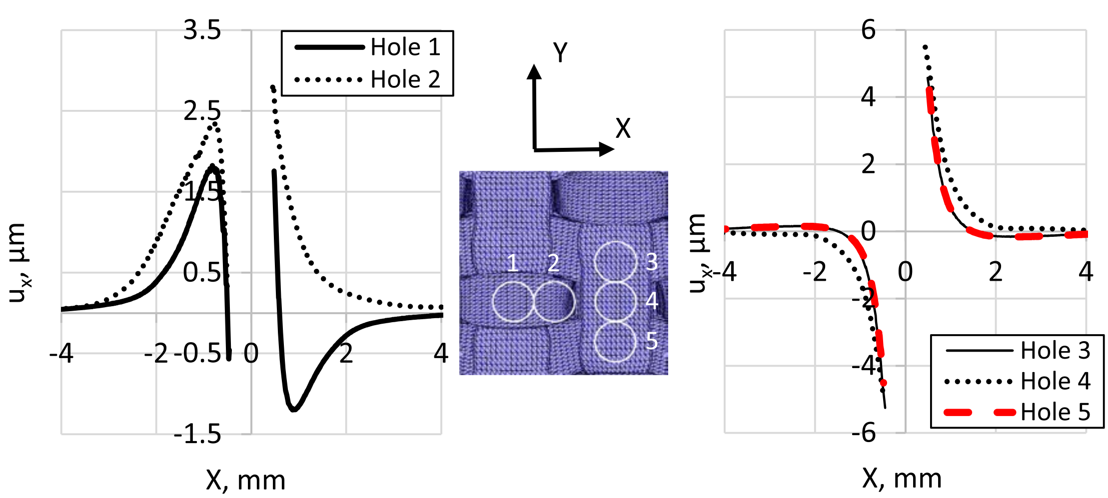

Fig. 5. Slice plots of displacements in warp direction (u_x) for the orthogonal reinforcement. (For interpretation of the references to colour in this figure legend, the reader is referred to the web version of this article.)

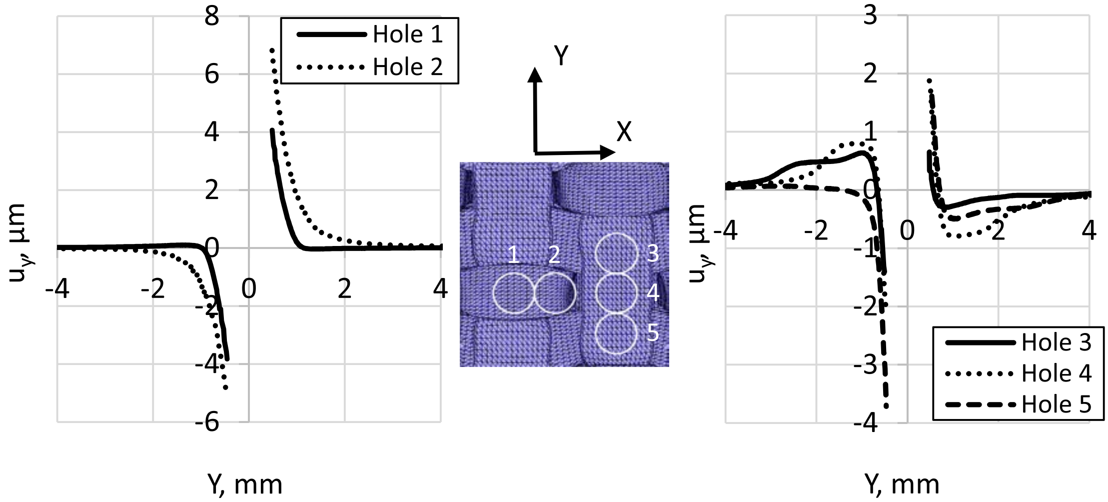

Fig. 6. Slice plots of displacements in weft direction (u_y) for the orthogonal reinforcement. (For interpretation of the references to colour in this figure legend, the reader is referred to the web version of this article.)

addition to closure it also shifts towards the crossing tow. This phenomenon can be explained by the tensile stress in X direction in the crossing weft.

Fig. 8 shows displacements in the weft direction. It is seen that these displacements are sensitive to the location only in the case of *hole* 1 through *hole* 3. The same trend is observed here as for the warp direction, namely, holes open transversely to the tows and close in the direction along their center line.

To summarize, our simulations show that the displacement fields around the drilled hole due to the residual stresses are noticeably sensitive to the hole location. Generally, in the direction transverse to the cut tow's central line, the hole opens due to the tensile residual stress in the surrounding resin. In the direction along the central line of the tow, the hole tends to close due to the prevailing longitudinal compressive residual stress. In the case when the hole is located at the intersection of the tows, it closes along the cut tow and shifts towards the crossing one. Thus, for the purpose of the interpretation of experimental data, the hole locations have to be chosen very accurately so the proper correlation can be made.

4.3. Hole depth dependence

In this section, we examine how residual-stresses-driven displacements on the surface of the specimen depend on the depth of the hole. For this purpose, several hole locations were chosen in both orthogonal and ply-to-ply reinforcement architectures and the hole depths was increased step by step in order to see how the displacements around the hole vary.

Simulations were performed for hole locations 3 and 5 in the ply-to-ply and 1 and 4 in the orthogonal specimens (see Fig. 4). The depths of each hole was gradually increased with a step of 0.5 mm, and the displacements were captured at the points located one hole radius away

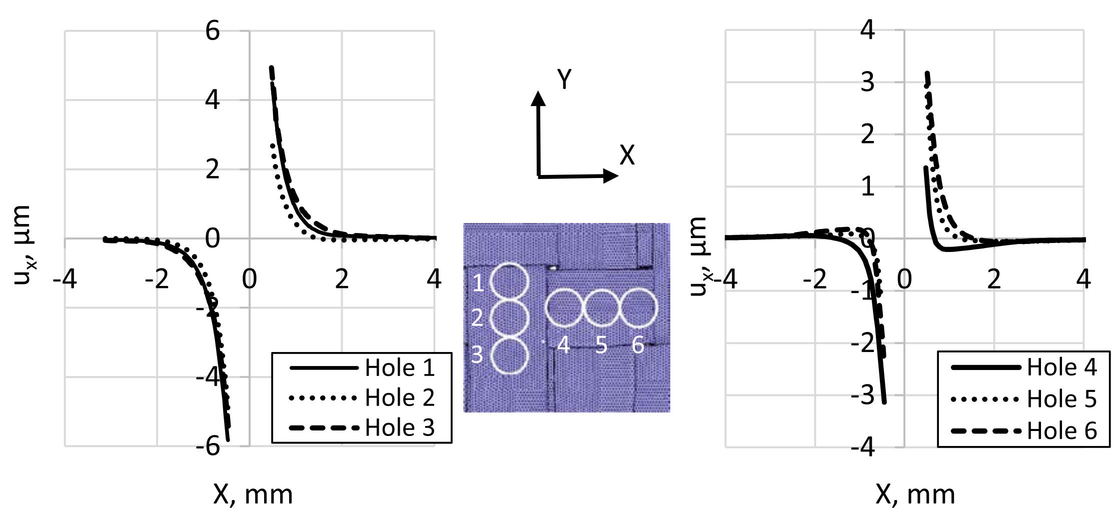

Fig. 7. Slice plots of displacements in warp direction (u_x) the ply-to-ply reinforcement. (For interpretation of the references to colour in this figure legend, the reader is referred to the web version of this article.)

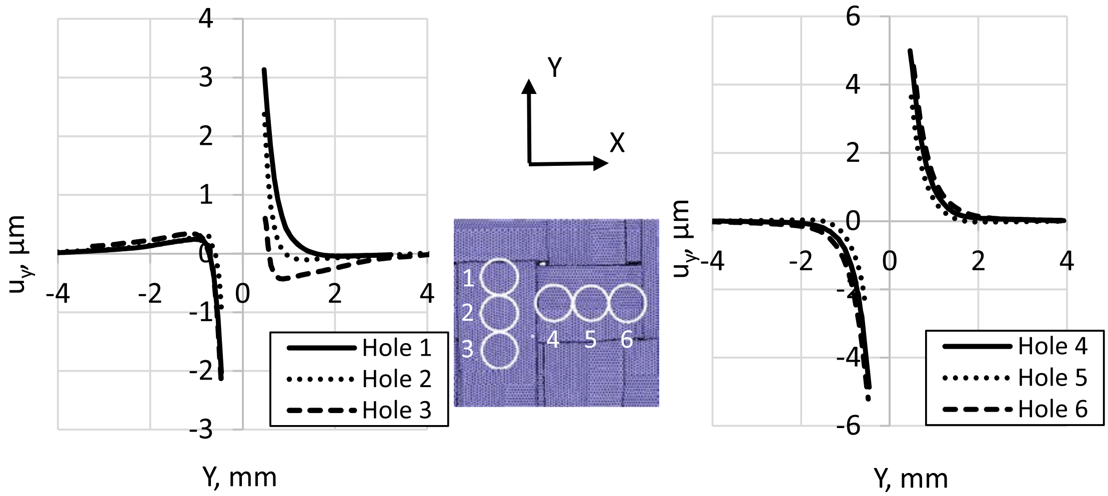

Fig. 8. Slice plots of displacements in weft direction (u_y) for the ply-to-ply reinforcement. (For interpretation of the references to colour in this figure legend, the reader is referred to the web version of this article.)

from the hole edge. The monitored points are denoted as white circles with numbers in Figs. 9–12. Each curve corresponds to the displacement of the point as a function of the hole depth.

It is seen in Figs. 9 and 10 that for the orthogonal reinforcement, the sensitivity to the depth is observed up to the hole depth of 2 mm which is the middle of the specimen panel thickness. In Fig. 9, it is seen that the hole opens more as the depth increases. This is dictated by the tensile residual stress in the epoxy resin in the direction transverse to the weft tow. The more weft tows are cut, the more pronounced the opening effect becomes.

In contrast, Fig. 10 shows that when the binder tow is cut ($H = 0.5mm$), the closure of the hole in the direction of the tow and slight opening in the transverse direction are observed. However, as the hole depth is increased, more and more weft tows under the binder are cut and the opening effect described for the previous hole location becomes dominant. This means that two competing effects compensate each other with the increasing depth and this can lead to a low level of displacements around the hole (Fig. 10) which can cause difficulties in the measurements because of insufficient resolution of an experimental method.

Figs. 11 and 12 show displacements in warp and weft directions depending on the hole depth in the ply-to-ply composite. It is seen that for this particular reinforcement architecture, the dependence on the hole depth is small comparing to the orthogonal reinforcement. This is due to the fact that perpendicular warps and wefts are cut sequentially as the hole depth increases, thus the opening and closing of the hole are balanced.

5. Interpretation of hole drilling results with FEA

This section describes how we used linear elastic mesoscale FEA models of drilling experiments to evaluate distributions of the residual stresses in carbon/epoxy composite panels with different 3D woven reinforcement architectures. The thermal mismatch stresses may cause

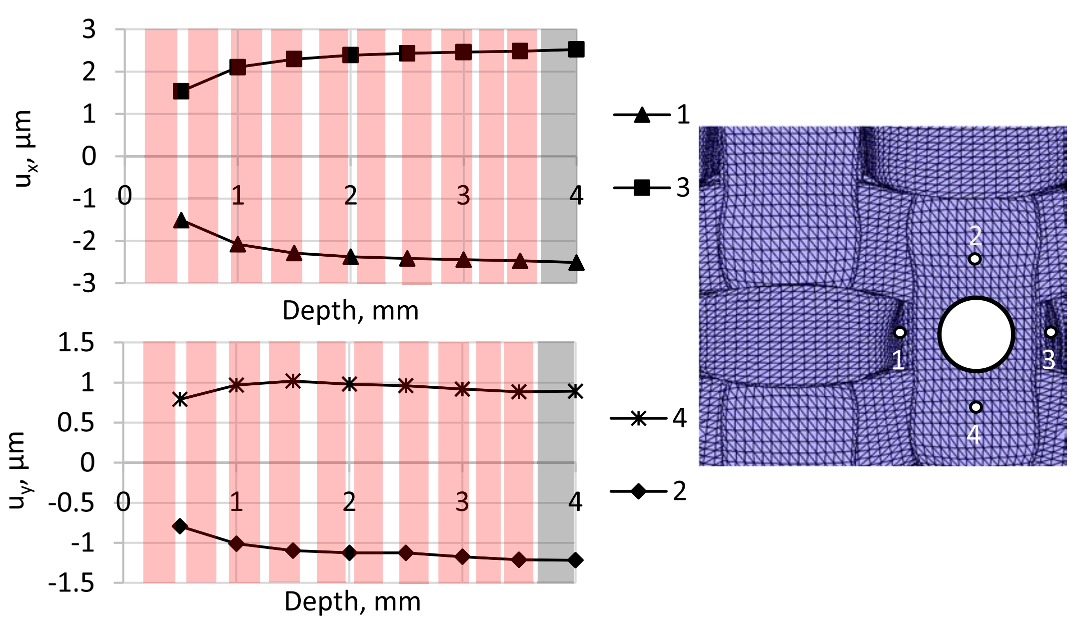

Fig. 9. Displacements in warp (u_x) and weft (u_y) directions at the points around *hole* 3 in the orthogonally reinforced composite as functions of the hole depth. In the plots, white background represents resin matrix, magenta stripes represent weft tows and grey stripes represent binder tows. (For interpretation of the references to colour in this figure legend, the reader is referred to the web version of this article.)

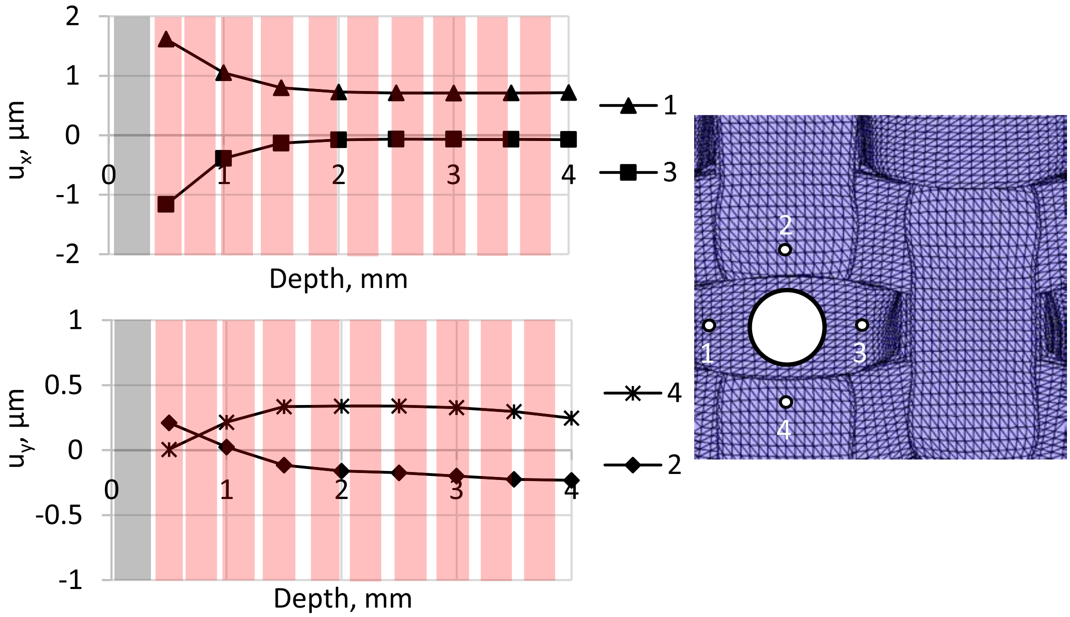

Fig. 10. Displacements in warp (u_x) and weft (u_y) directions at the points around *hole* 1 in the orthogonally reinforced composite as functions of the hole depth. In the plots, white background represents resin matrix, magenta stripes represent weft tows and grey stripes represent binder tows. (For interpretation of the references to colour in this figure legend, the reader is referred to the web version of this article.)

viscoelastic or plastic deformation, so the assumption of linear elasticity may lead to overestimation of residual stresses. In some extreme cases the matrix can even microcrack to accommodate the residual stresses, see [11] To account for those complex effects without overcomplicating the models, we propose a simple approximate approach to interpret the experimental measurements. Instead of simulating the actual temperature interval ΔT from the curing to room temperature, we determine the equivalent temperature drop ΔT^{eff} that corresponds to the surface displacements experimentally observed in the specimens after hole drilling. This ΔT^{eff} is smaller than ΔT and is different for different material systems and reinforcement architectures.

The procedure to find ΔT^{eff} is as follows. First, the initial simulation of cooling after curing is run with the actual ΔT. After that the drilling process is simulated by removing the corresponding elements and the displacements of the surface points are observed. Then the values of the numerically predicted displacements at the points approximately one radius away from the hole boundary are selected to compare with the experimental measurements (note that the approach of considering a set of points at a certain distance from the hole edge is similar to the one used in [17]). The adjustment coefficient k_{eff} is found as the ratio of the average experimental displacement to the average displacement from the initial model in the corresponding points. Then the simulation

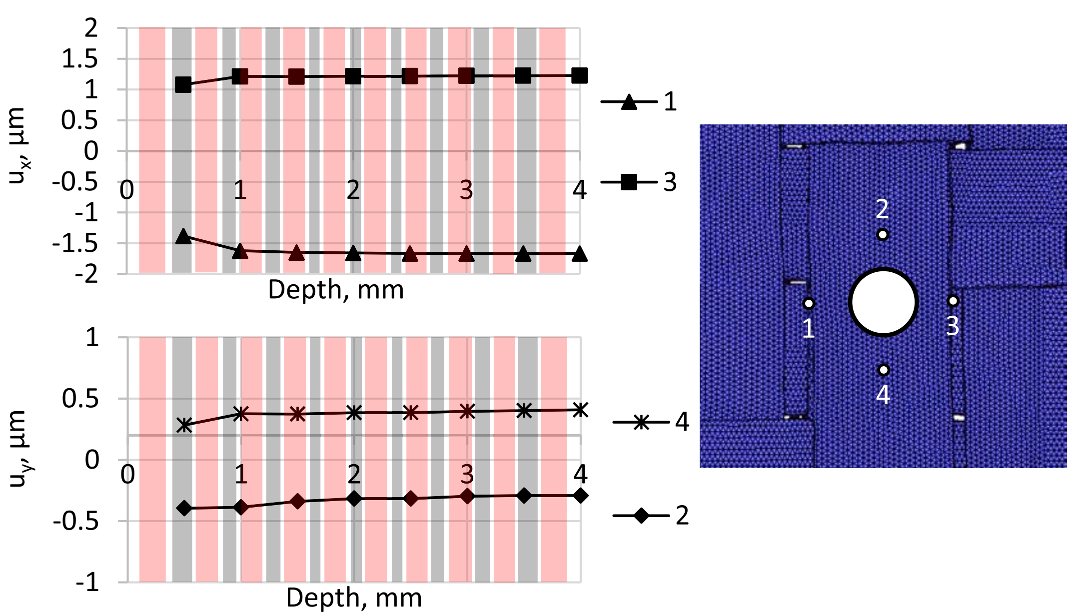

Fig. 11. Displacements in warp (u_x) and weft (u_y) directions at the points around *hole* 3 in ply-to-ply composite as functions of the hole depth. In the plots, white background represents resin matrix, magenta stripes represent weft tows and grey stripes represent warp tows. (For interpretation of the references to colour in this figure legend, the reader is referred to the web version of this article.)

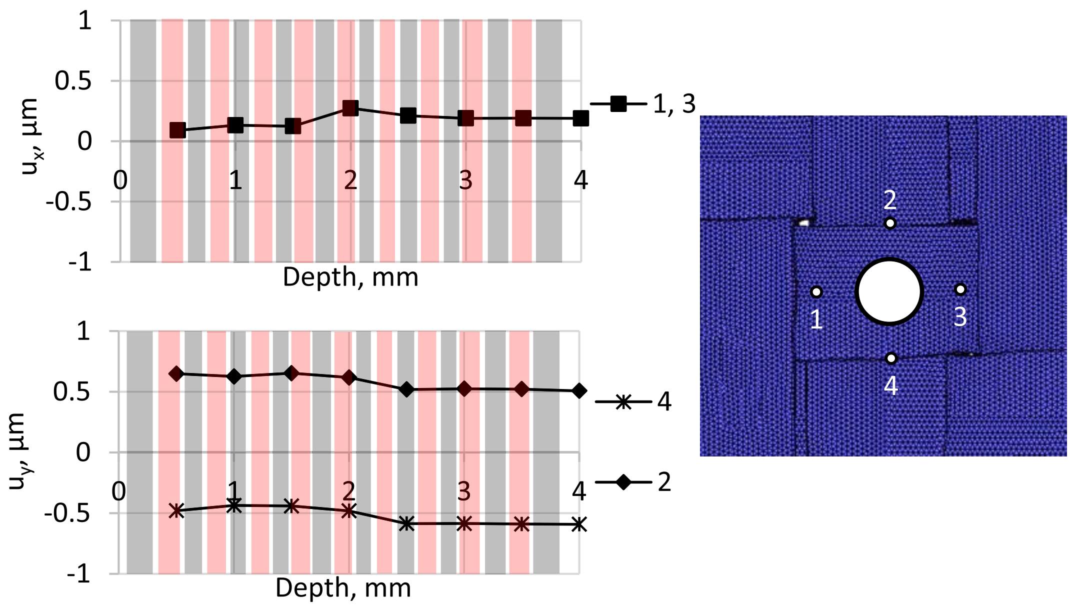

Fig. 12. Displacements in warp (u_x) and weft (u_y) directions at the points around *hole* 5 in ply-to-ply composite as functions of the hole depth. The curve for point 1 coincides with the curve for point 3. In the plots, white background represents resin matrix, magenta stripes represent weft tows and grey stripes represent warp tows. (For interpretation of the references to colour in this figure legend, the reader is referred to the web version of this article.)

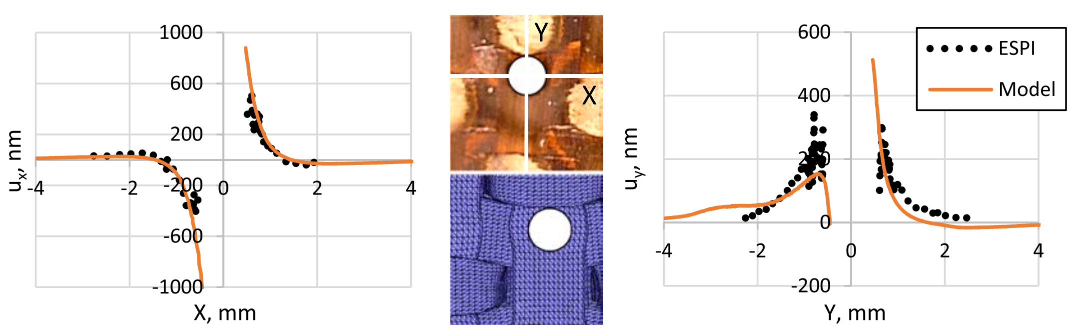

Fig. 13. Displacement in warp (u_x) and weft (u_y) directions around the hole cutting the weft tow in the orthogonally reinforced composite. $\Delta T^{eff} = -30$ °C. (For interpretation of the references to colour in this figure legend, the reader is referred to the web version of this article.)

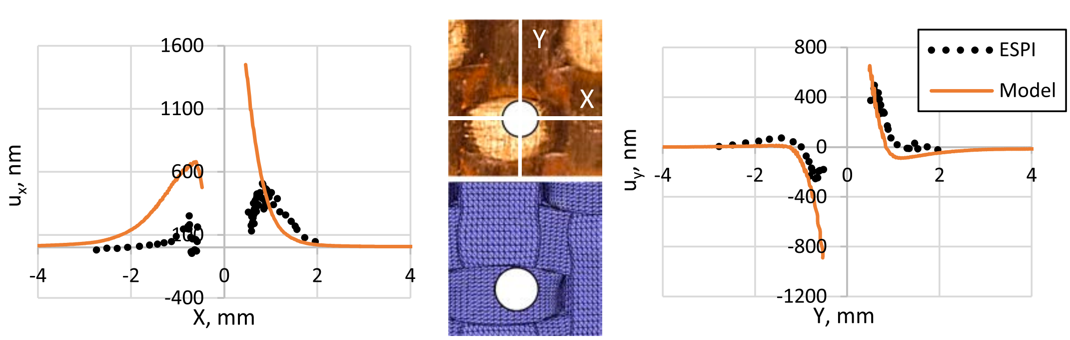

Fig. 14. Displacement in warp (u_x) and weft (u_y) directions around the hole cutting the binder tow in the orthogonally reinforced composite. $\Delta T^{eff} = -30$ °C. (For interpretation of the references to colour in this figure legend, the reader is referred to the web version of this article.)

of cooling by $\Delta T^{eff} = k_{eff}\Delta T$ is performed to produce the approximate distribution of the cure-induced residual stresses. Note that dependence of the predicted residual stresses on ΔT is not exactly linear since thermo-mechanical properties of epoxy are modeled as temperature-dependent. In the equivalent numerical simulations we assume that the temperature drop starts from the curing temperature.

Figs. 13–15 present examples of the experimentally observed and numerically predicted displacements due to blind hole drilling in 3 particular locations of the orthogonally reinforced composite: in the weft tow, in the binder tow, and in the matrix. Table 3 provides coordinates of the hole centers in the corresponding unit cell coordinate systems. The hole depth is $0.5mm$ so that it penetrates up to 2 tows, depending on the location. All of the simulations for this particular architecture were performed with the same adjustment coefficient $k_{eff} = 0.214$ resulting in $\Delta T^{eff} = -30$ °C. As can be seen, the ΔT^{eff} approach shows good correspondence between numerical and experimental data for the displacements perpendicular to the tow direction and for the hole in the matrix. The correspondence for the displacements along the tow is not as good. We observe significant differences between the warp-direction displacements due to the hole in the binder

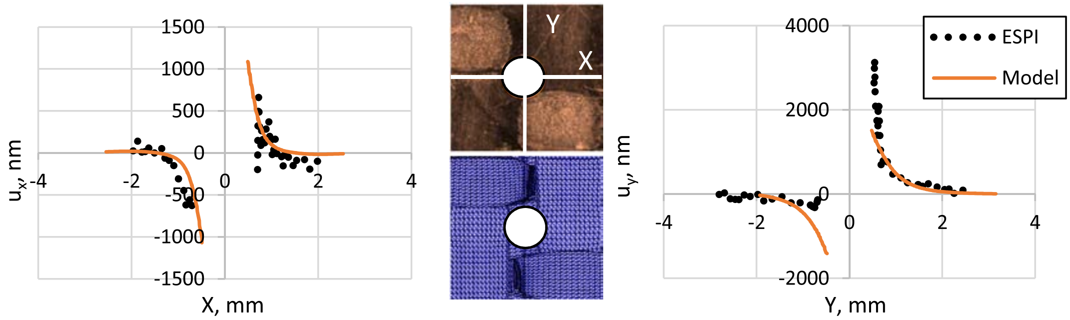

Fig. 15. Displacement in warp (u_x) and weft (u_y) directions around the hole drilled in the epoxy resin matrix for the orthogonally reinforced composite. $\Delta T^{eff} = -30$ °C. (For interpretation of the references to colour in this figure legend, the reader is referred to the web version of this article.)

Table 3
Coordinates of the centers of the holes drilled in the weft, warp, binder and resin constituents of the composites.

	Orthogonal reinforcement			Ply-to-ply reinforcement	
	Weft	Binder	Resin	Warp	Weft
X, mm	3.81	1.71	2.54	5.52	2.83
Y, mm	3.22	1.95	3.15	4.54	2.65

and the weft-direction displacements around the hole cutting the weft tow. Most likely, these discrepancies are due to the local interactions of the reinforcing tows that are difficult to capture both experimentally (small values or large gradients in the displacements) and numerically (numerical model requires a layer of resin material between tows). The second possible reason is that the nonlinear effects (plasticity, etc.) which we approximate by the adjustment coefficient in $\Delta T^{eff} = k_{eff}\Delta T$ can have different intensity in different directions and locations of the unit cell. Yet another possible reason is the inhomogeneity of the temperature distribution and degree of cure during the curing process.

The influence of local interactions can be seen in the predicted displacements u_y when cutting the weft tow, Fig. 13. The portion of the displacement field captured above the hole shows good agreement with the experiment whereas the portion from below the hole is noticeably different. This can be explained by the fact that the hole cuts the weft tow near the crossing binder (above the hole). The behavior of the

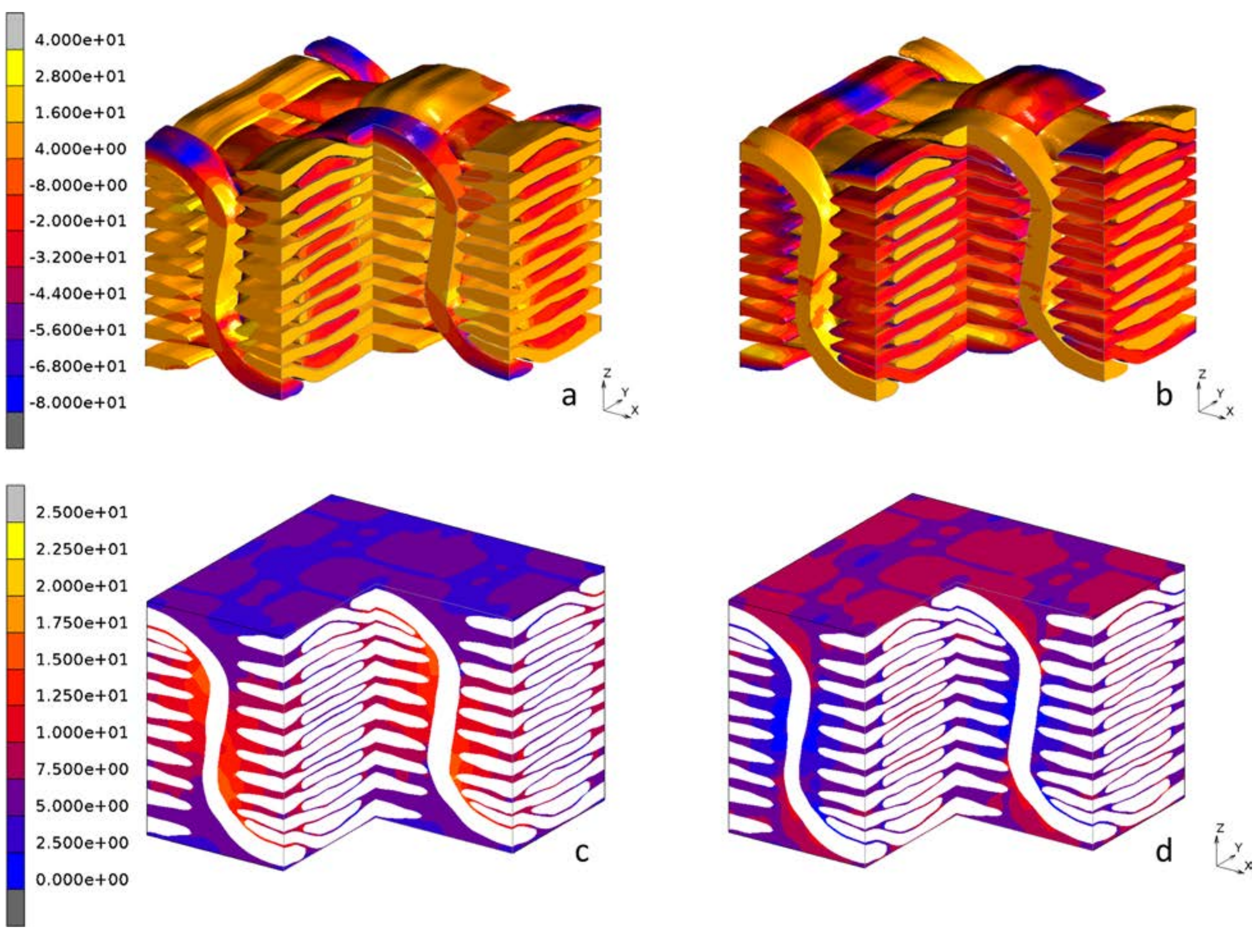

Fig. 16. Manufacturing-induced residual stress distribution in the orthogonally reinforced composite for $\Delta T^{eff} = -30$ °C. (a) Normal stress σ_{xx} in the warp direction accumulated in the tows, (b) normal stress σ_{yy} in the weft direction in the tows, (c) hydrostatic stress in the epoxy, and (d) Von Mises stress in the epoxy. All values are in MPa. (For interpretation of the references to colour in this figure legend, the reader is referred to the web version of this article.)

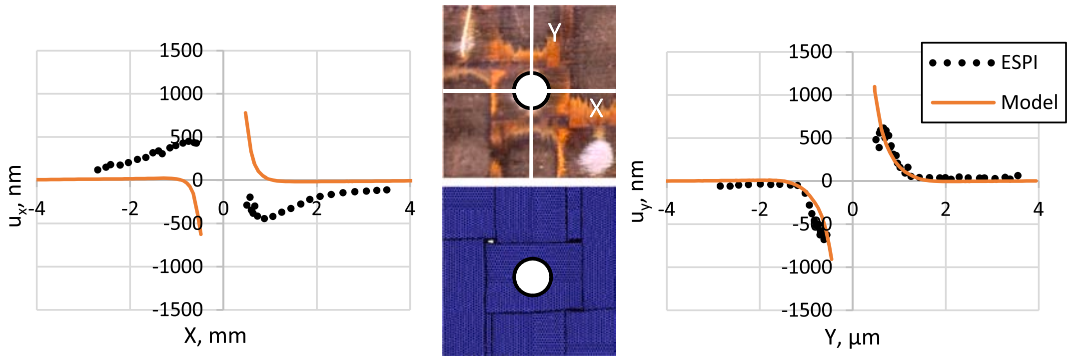

Fig. 17. Displacement in warp (u_x) and weft (u_y) directions around the hole cutting the warp tow of the ply-to-ply composite. $\Delta T^{eff} = -40$ °C. (For interpretation of the references to colour in this figure legend, the reader is referred to the web version of this article.)

material on top of the binder tow in the weft direction would have a greater impact from the tensile residual stress in the resin and also from the binder tow. The weft (Y) direction of the specimen is collinear with the transverse direction of the crossing binder tow above the hole and as stated previously, the transverse residual stresses in the tows are tensile so the upper portion of the hole edge is subjected to the tensile residual stress. This observation proves that the model predicts the behavior of the material with good accuracy when it is governed by the tensile stress in the resin. On the other hand, when the local behavior of the material is dictated by the residual longitudinal compressive stress in the tow, there are deviations between predictions and experimental measurements.

Figs. 14 and 15 also confirm that the model correlates with the experiments well when the behavior is governed by tensile residual stress in the epoxy including the displacement u_y for the hole in the binder and both displacements for the hole in the resin. The warp displacement curves in Fig. 14, both numerical and experimental, show the hole shifting towards a resin rich region to the right of the hole illustrating the ability of the proposed approach to capture the mechanics of the material deformation.

Overall, it appears that most of the experimentally observed surface displacements caused by drilling of blind $0.5mm$ holes in the considered composite are well predicted (both qualitatively and quantitatively) by the simulations of the residual stresses due to cooling by an effective temperature drop ΔT^{eff}. This observation allows us to obtain an approximate prediction of the distribution of residual stresses in the entire unit cell of the composite. As an illustration, Fig. 16 presents distribution of the warp-direction and weft-direction components of the stress in the tows, and hydrostatic and Von Mises equivalent stresses in the matrix. The actual ranges of the stresses are -158 MPa $\le \sigma_{xx} \le 50$ MPa, -112 MPa $\le \sigma_{yy} \le 26$ MPa in the tows, and -4.5 MPa $\le \sigma_H \le 25$ MPa, $\sigma_{VM} \le 25$ MPa in the matrix, however the stress concentrations are very localized so different bounds were selected in the plots for better presentation of stress distribution. Note that concentrations of hydrostatic residual stresses in the resin of orthogonally reinforced woven composites have been shown to correlate with the manufacturing-induced microcracking, see [31].

Similar analysis was performed for the ply-to-ply reinforced composite. The holes of 0.5 mm depths were drilled in two locations on the surface of the specimen: cutting a warp tow (Fig. 17) and cutting a weft tow (Fig. 18), see Table 3. For this particular material reinforcement architecture the adjustment coefficient k_{eff} was found to be equal to 0.286 leading to $\Delta T^{eff} \approx -40$ °C regardless of the hole location.

Figs. 17 and 18 show similar trends in the predictions as in the case of orthogonal reinforcement. The model with $\Delta T^{eff} \approx -40$ °C provides accurate estimates for the displacements perpendicularly to the tow while showing significant deviations for the displacements in the direction of the tow. The resulting prediction for distributions of the residual stresses in the entire unit cell are presented in Fig. 19. The range of the predicted stresses is -48 MPa $\le \sigma_{xx} \le 15$ MPa, -65 MPa $\le \sigma_{yy} \le 15$ MPa in the tows, and -0.3 MPa $\le \sigma_H \le 17$ MPa, 2.4 MPa $\le \sigma_{VM} \le 16$ MPa in the matrix. As expected the manufacturing-induced residual stresses in the ply-to-ply reinforced composites are lower than in the case of orthogonal reinforcement, since their residual stresses can be released by deformation in the through-thickness direction.

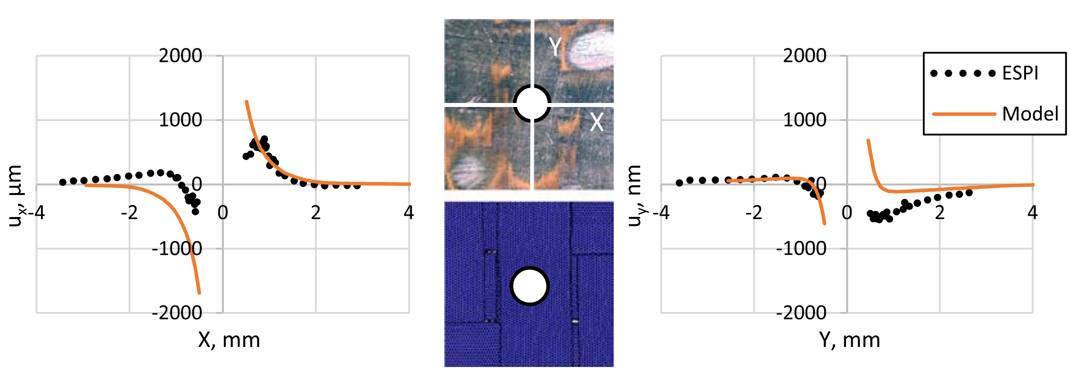

Fig. 18. Displacement in warp (u_x) and weft (u_y) directions around the hole cutting the weft tow of the ply-to-ply composite. $\Delta T^{eff} = -40$ °C. (For interpretation of the references to colour in this figure legend, the reader is referred to the web version of this article.)

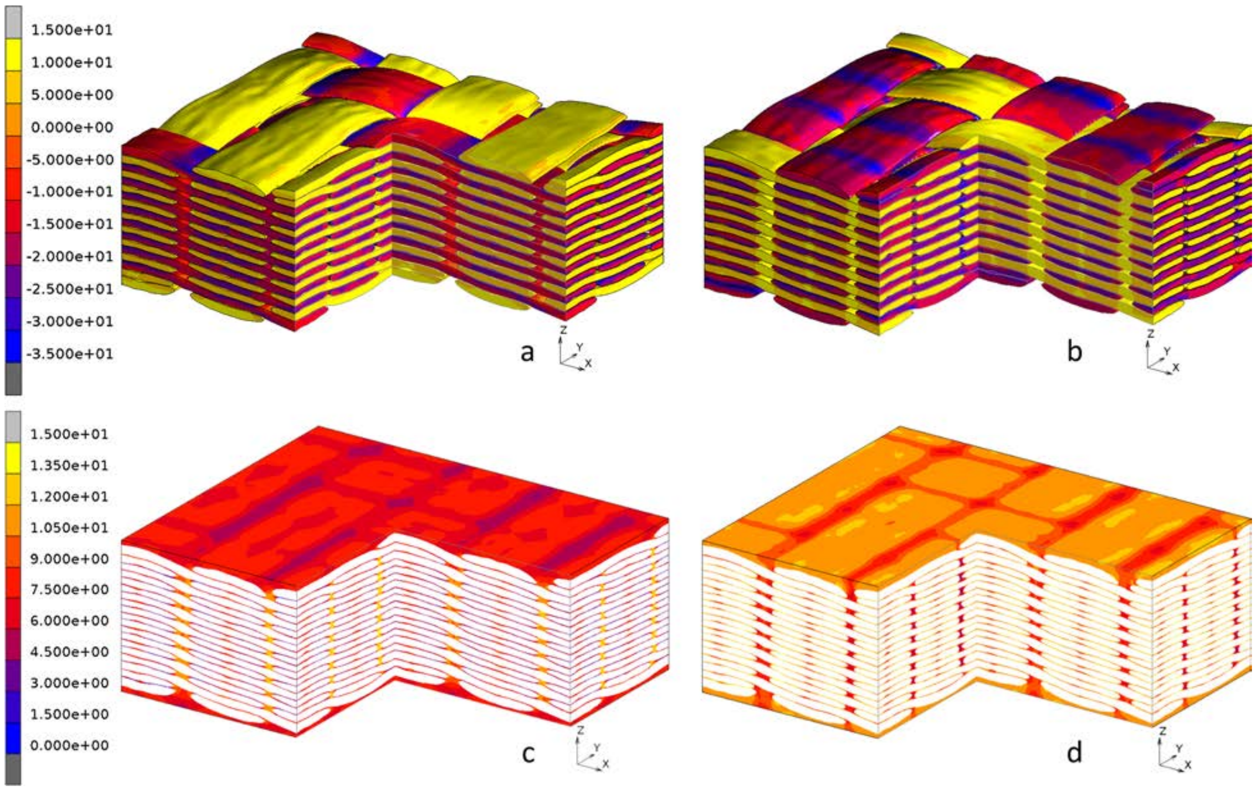

Fig. 19. Manufacturing-induced residual stress distribution in the ply-to-ply reinforced composite for $\Delta T^{eff} = -40$ °C. (a) Normal stress σ_{xx} in the warp direction accumulated in the tows, (b) normal stress σ_{yy} in the weft direction in the tows, (c) hydrostatic stress in the epoxy, and (d) von Mises stress in the epoxy. All values are in MPa. (For interpretation of the references to colour in this figure legend, the reader is referred to the web version of this article.)

6. Conclusions

Mesoscale FE models can be used to interpret hole drilling experimental data and obtain spatial distribution of curing-induced residual stresses in 3D woven carbon/epoxy composites. It has been shown that the surface displacements around the hole are sensitive to the hole location with respect to the composite reinforcement. It has also been observed that the residual-stress-release related displacements depend on the hole depth and can become too small and difficult to measure for certain hole depth values. This phenomenon can be explained by the competing residual stresses in the composite material, namely the tensile residual stress in the epoxy resin matrix and the longitudinal compressive stress in the tows. The interaction between the tows and resin contribute to the complexity of the local residual stress distribution.

Nonlinear behavior of the resin during cooling after curing is included in the linear elastic models by selecting an adjusted temperature drop ΔT^{eff} determined from the processing of experimental ESPI data. The ΔT^{eff} was found to have the same value for different hole locations in the same material but different values for different material reinforcement architectures. The consistency of the value for the same architecture suggests that the proposed simplified approach can be used as a good first-order estimate for the residual stress distribution. The observation that different materials have different consistent values of ΔT^{eff} shows that the level of nonlinearity in the material behavior during manufacturing varies for different composite reinforcement architectures.

Declaration of Competing Interest

The authors declare that they have no known competing financial interests or personal relationships that could have appeared to influence the work reported in this paper.

Acknowledgements

This material is based upon work supported by the National Science Foundation, USA through grant CMMI-1662098. The authors acknowledge participation of Adam Ewert in the development of finite element models.

References

[1] Bogetti TA, Gillespie JW. Process-induced stress and deformation in thick-section thermoset composite laminates. J Compos Mater 1992;26:626–60. https://doi.org/10.1177/002199839202600502.
[2] Li M, Tucker CL. Modeling and simulation of two-dimensional consolidation for thermoset matrix composites. Compos –Part A Appl Sci Manuf 2002;33:877–92. https://doi.org/10.1016/S1359-835X(02)00017-9.
[3] Cowley KD, Beaumont PWR. The measurement and prediction of residual stresses in carbon-fibre/polymer composites. Compos Sci Technol 1997;57:1445–55. https://doi.org/10.1016/S0266-3538(97)00048-1.
[4] Wisnom MR, Gigliotti M, Ersoy N, Campbell M, Potter KD. Mechanisms generating residual stresses and distortion during manufacture of polymer-matrix composite structures. Compos Part A Appl Sci Manuf 2006;37:522–9. https://doi.org/10.1016/j.compositesa.2005.05.019.
[5] Maier G, Hofmann F. Performance enhancements of polymer-matrix composites by changing of residual stresses. Compos Sci Technol 2008;68:2056–65. https://doi.org/10.1016/j.compscitech.2008.03.001.
[6] Kim YK. Process-induced residual stress analysis by resin transfer molding. J Compos Mater 2004;38:959–72. https://doi.org/10.1177/0021998304043746.
[7] Golestanian H, El-Gizawy AS. Modeling of process induced residual stresses in resin transfer molded composites with woven fiber mats. J Compos Mater 2001;35:1513–28. https://doi.org/10.1106/VW5C-GN89-UXKR-WFKT.
[8] Fiedler B, Hojo M, Ochiai S. The influence of thermal residual stresses on the transverse strength of CFRP using FEM. Compos Part A Appl Sci Manuf 2002;33:1323–6. https://doi.org/10.1016/S1359-835X(02)00169-0.
[9] Agius SL, Joosten M, Trippit B, Wang CH, Hilditch T. Rapidly cured epoxy/anhydride composites: effect of residual stress on laminate shear strength. Compos Part A Appl Sci Manuf 2016;90:125–36. https://doi.org/10.1016/j.compositesa.2016.06.013.
[10] Benavente M, Marcin L, Courtois A, Lévesque M, Ruiz E. Numerical analysis of viscoelastic process-induced residual distortions during manufacturing and post-curing. Compos Part A Appl Sci Manuf 2018;107:205–16. https://doi.org/10.1016/

j.compositesa.2018.01.005.

[11] Tsukrov I, Bayraktar H, Giovinazzo M, Goering J, Gross T, Fruscello M, et al. Finite element modeling to predict cure-induced microcracking in three-dimensional woven composites. Int J Fract 2011;172:209–16. https://doi.org/10.1007/s10704-011-9659-x.

[12] Schajer GS, Yang L. Residual-stress measurement in orthotropic materials using the hole-drilling method. Exp Mech 1994;34:324–33. https://doi.org/10.1007/BF02325147.

[13] Pagliaro P, Zuccarello B. Residual stress analysis of orthotropic materials by the through-hole drilling method. Exp Mech 2007;47:217–36. https://doi.org/10.1007/s11340-006-9019-3.

[14] Pisarev V, Eleonsky SI, Chernov AV. Residual stress characterization in orthotropic plate by combining hole-drilling method and speckle interferometry. 29th Congr. Int. Counc. Aeronaut. Sci.. 2014.

[15] Lekhnitskii SG. Theory of Elasticity of an Anisotropic Elastic Body. Holden-Day; 1963.

[16] Akbari S, Taheri-Behrooz F, Shokrieh MM. Characterization of residual stresses in a thin-walled filament wound carbon/epoxy ring using incremental hole drilling method. Compos Sci Technol 2014;94:8–15. https://doi.org/10.1016/j.compscitech.2014.01.008.

[17] Wu LF, Zhu JG, Xie HM. Investigation of residual stress in 2D plane weave aramid fibre composite plates using moiré interferometry and hole-drilling technique. Strain 2015;51:429–43. https://doi.org/10.1111/str.12155.

[18] Gross T, Buntrock H, Tsukrov I, Drach B, Vasylevskyi K, Chagnon N. Measurement of intrinsic residual stresses in 3D woven composites using measurement of the displacement fields from hole drilling by electronic speckle pattern interferometry and digital image correlation. Am Soc Compos 2018;2018. https://doi.org/10.12783/asc33/26127.

[19] Díaz F, Kaufmann G, Galizzi G. Determination of residual stresses using hole drilling and digital speckle pattern interferometry with automated data analysis. Opt Lasers Eng 2000;33:39–48. https://doi.org/10.1016/S0143-8166(00)00022-1.

[20] Drach A, Drach B, Tsukrov I. Processing of fiber architecture data for finite element modeling of 3D woven composites. Adv Eng Softw 2014;72:18–27. https://doi.org/10.1016/j.advengsoft.2013.06.006.

[21] Wang Y, Sun X. Digital-element simulation of textile processes. Compos Sci Technol 2001;61:311–9. https://doi.org/10.1016/S0266-3538(00)00223-2.

[22] Lomov SV, Ivanov DS, Verpoest I, Zako M. Meso-FE modelling of textile composites : Road map, data flow and algorithms. Compos Sci Technol 2007;67:1870–91. https://doi.org/10.1016/j.compscitech.2006.10.017.

[23] Zhou E, Mollenhauer D, Iarve E. A realistic 3-D textile geometric model. Seventeenth Int. Conf. Compos. Mater. ICCM-17. 2009. p. 100–10.

[24] Long AC, Brown LP. 8 - Modelling the geometry of textile reinforcements for composites: TexGen. In: Boisse P, editor. Compos. Reinf. Optim. Perform. Woodhead Publishing; 2011. p. 239–64. https://doi.org/10.1533/9780857093714.2.239.

[25] Miao Y, Zhou E, Wang Y, Cheeseman BA. Mechanics of textile composites: Micro-geometry. Compos Sci Technol 2008;68:1671–8. https://doi.org/10.1016/j.compscitech.2008.02.018.

[26] Ewert A, Drach B, Vasylevskyi K, Tsukrov I. Predicting the overall response of an orthogonal 3D woven composite using simulated and tomography-derived geometry. Compos Struct 2019.

[27] Whitcomb JD, Chapman CD, Tang X. Derivation of boundary conditions for micromechanics analyses of plain and satin weave composites. J Compos Mater 2000;34:724–47. https://doi.org/10.1177/002199830003400901.

[28] Tsukrov I, Giovinazzo M, Vyshenska K, Bayraktar H, Goering J, Gross T. Comparison of two approaches to model cure-induced microcracking in three-dimensional woven composites. In: Vol. 3 Des. Mater. Manuf. Parts A, B, C, ASME; 2012. p. 541. https://doi.org/10.1115/IMECE2012-86395.

[29] Tsukrov I, Vasylevskyi K, Drach B, Buntrock H, Gross T. Utilizing numerical models to identify process-induced residual stresses in 3D woven carbon/epoxy composites. IOP Conf. Ser. Mater. Sci. Eng. 2018. https://doi.org/10.1088/1757-899X/406/1/012030.

[30] Brauner C, Block TB, Purol H, Herrmann AS. Microlevel manufacturing process simulation of carbon fiber/epoxy composites to analyze the effect of chemical and thermal induced residual stresses. J Compos Mater 2012;46:2123–43. https://doi.org/10.1177/0021998311430157.

[31] Drach B, Tsukrov I, Trofimov A, Gross T, Drach A. Comparison of stress-based failure criteria for prediction of curing induced damage in 3D woven composites. Compos Struct 2018;189:366–77. https://doi.org/10.1016/j.compstruct.2018.01.057.